Finite element simulations of the double-diaphragm forming process

Comparisons with experimental trials

Xiaobo Yu* — Lin Ye* — Yiu-Wing Mai* — Bruce Cartwright
Damian McGuckin** — Rowan Paton*****

** School of Aerospace, Mechanical and Mechatronic Engineering*
The University of Sydney
NSW 2006 Australia

{xiaobo.yu; ye, mai}@aeromech.usyd.edu.au

*** Pacific Engineering Systems International Pty Ltd*
Unit 22, 8 Campbell Street, Artarmon
NSW 2064 Australia

{Brucec, damianm}@esi.com.au

**** Cooperative Research Centre for Advanced Composite Structures (CRC-ACS)*
506 Lorimer Street, Fishermans Bend
VIC 3207 Australia

r.paton@crc-acs.com.au

ABSTRACT. *This document provides a comprehensive evaluation of finite element simulations of double diaphragm forming of CF/EP plain weave prepreg. The simulations were performed using the PAM-FORM software, and incorporated critical advances recently achieved in composite forming simulations. The material properties were obtained from characterization tests, or estimated in conjunction with rationalization analyses. By using only one set of material and simulation parameters, the best-match simulations correlate well with all four experimental trials of different setups, which include one good and one wrinkled forming trail of rudder rib shape, and one good and one wrinkled forming trial of a simple cup shape. The simulations also highlight the effects of contact penalty, and the sensitivity to inter-ply friction, and re-confirm the necessity to scale-up the measured intra-ply shearing stiffness.*

KEYWORDS: *diaphragm forming, finite element simulation, experimental verification.*

REEF – 14/2005. Composites forming simulation, pages 633 to 651

1. Introduction

Carbon fibre reinforced epoxy composites are well accepted in the aerospace industry. Traditionally, they are formed by successive hand lamination of individual plies. This is appropriate and efficient for small production runs, but makes composite parts too expensive for high-volume production (Young, 2003).

To achieve automation and reduce manufacturing costs, aerospace industries and research institutes around the world have been developing alternative manufacturing approaches, such as resin transfer moulding, resin infusion, stamping and diaphragm forming processes. For the purpose of quickly identifying optimum parameters for these processes, numerical simulations are also in development. In respect to the stamping, draping or diaphragm forming processes, two simulation approaches are commonly applied. One is kinematical analysis, (*e.g.* VanWest *et al*., 1991; Laroche *et al*., 1994; Long *et al*., 2002), which considers the final geometry of the formed part, the fibre locking angle, and recently the effects of fibre architecture as well. This method is fast and capable of predicting the formability of a single ply. The other is mechanical or finite element (FE) analysis, (*e.g.* de Luca *et al*., 1998; Dong *et al*., 2001; Boisse *et al*., 2001; Cao *et al*., 2003), which considers more parameters, such as boundary conditions, material constitutions, forming rate, and interface frictions. The finite element technique is slower, but has the potential to predict the quality of, or the process windows for, forming a multi-ply component.

This study concerns the approach of FE analysis, and the process of double diaphragm forming of woven fabrics impregnated with epoxy resin. Diaphragm forming has been identified and developed, by CRC-ACS, to be the leading solution to automated preforming of a large variety of aerospace parts, which are subsequently assembled into completed structure (Mair, 2002).

The work presented in this paper is based on a commercial FE package PAM-FORM (ESI software, 2002). Early trials of PAM-FORM simulations on diaphragm forming have been presented (Yu *et al*., 2000). Since then, a number of advances have been achieved in FE analysis, which include a better understanding of diaphragm properties, improved FE treatment of intra-ply shearing stiffness (Yu *et al*., 2003a), more accurate experimental data (Yu, 2003) and modelling (Cartwright *et al*., 2003) of inter-ply friction. A recent and critical advance is the discovery of, and a remedy to, the spurious wrinkles and the underlying numerical locking phenomenon specific to fibre reinforced composites (Yu *et al*., 2004a; 2004b), and consequently the awareness of possible effects of compaction pressure on intra-ply shearing stiffness and a related back-calculation approach (Yu *et al*., 2004c). These advances cover most essential aspects, from characterisation and modelling of material properties, to fundamental theory and basic principles of FE method, in developing diaphragm forming simulations.

The purpose of this study is to establish a comprehensive evaluation of the diaphragm forming simulations following these advances. Such an evaluation,

which was previously not available, is essential for aerospace industry to accept finite element analysis as a designing tool in developing a practical diaphragm forming process.

2. Double diaphragm forming process and experimental trials

The double-diaphragm forming process has been documented in a number of CRC-ACS reports up to date (*e.g.* Bibo *et al.*, 2000; Young, 2003). In brief, a typical double diaphragm forming process consists of three steps as schematically illustrated in Figure 1. In the first step, a flat fabric or tape stack, called a preform, is laid up according to the laminate design, and is placed between two diaphragms. The diaphragms are positioned and secured over a hollow forming box with forming tools beneath the preform. Full vacuum is then applied to the cavity between the diaphragms. In the cases where pre-impregnated fabrics or tapes, called prepregs, are used, the second step is to heat up the flat preform to assist the inter-ply and intra-ply shearing during subsequent forming. The final step is to evacuate the air volume beneath the bottom diaphragm and within the forming box at a controlled rate. The diaphragms are then pushed down by the atmospheric air pressure and forcing the fabric/tape stack to conform to the tool geometry. During this period the vacuum between the top and bottom diaphragm is sustained and the heat input continues. At the end of this step, the formed part is suitable for preparation for autoclave cure.

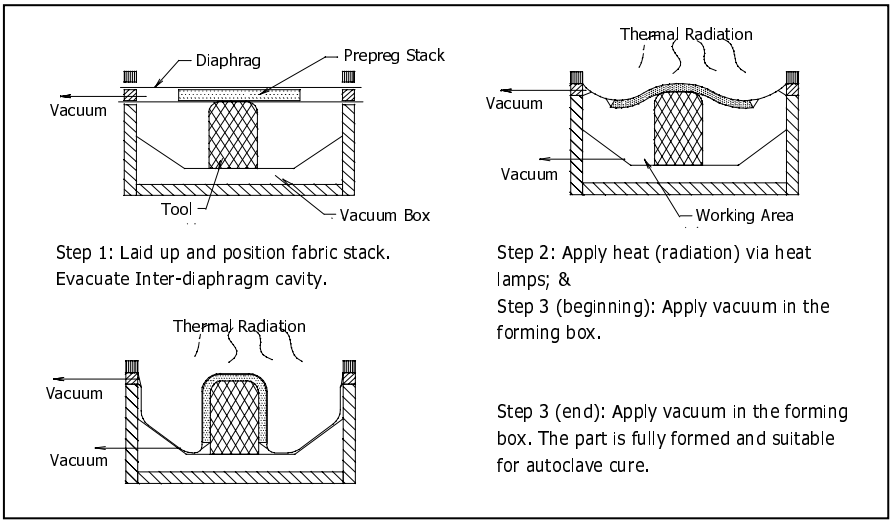

Figure 1. *Double diaphragm forming process [after (Bibo* et al., *2000)]*

Four experimental trials, as listed in Table 1, were simulated in this study. Trials 1 and 2 were performed on a typical aerospace part, a rudder leading edge rib as shown in Figure 2a. Full details of these two trials have been documented in (Crossthwaite *et al*., 2000). In brief, the part was formed in a rectangular box which was 725mm long, 425mm wide and 100mm deep, from a stack of 6-ply $[\pm 45, 0/90, \pm 45]_s$ carbon fibre plain weave epoxy prepreg (CF/EP). At the beginning of the forming process, the stack of prepreg was sandwiched into a double-diaphragm pack and was positioned immediately above the rib tool, as illustrated in Figure 2b. The setups and forming parameters of the two experimental trials were identical, except that different vacuum levels were applied between the diaphragms. In Exp. Trial 1, full factory vacuum, 95kPa, was applied. As a result, a good part was formed as demonstrated in Figure 2c. In Exp. Trial 2, partial vacuum, 38 kPa, was applied. Consequently, a wrinkled part was formed as shown in Figure 2d. In both trials, deformations in the top diaphragms were measured.

Table 1. *Four experimental trials of double diaphragm forming*

Exp. Trial ID	Part geometry	Inter-diaph vacuum	Ply lamination *	Forming quality
1	rudder rib	95 kPa	6-ply	good, Figure 2c
2	rudder rib	38 kPa	6-ply	wrinkled, Figure 2d
3	simple cup	95 kPa	6-ply	wrinkled, Figure 3b
4	simple cup	95 kPa	3-ply	good

* 6-ply: $[\pm 45, 0/90, \pm 45]_s$; 3-ply: $[\pm 45, 0/90, \pm 45]$.

Exp. Trials 3 and 4 were performed on forming an idealised geometry, a simple cup shape as shown in Figure 3. Full details of the trials have been documented in (Young *et al*., 2001). In brief, the part was formed in a round cavity which was 420mm in diameter and 100mm in depth, onto a cylindrical tool which was 100mm in diameter, from a stack of CF/EP prepreg which was the same material as used in Exp. Trials 1 and 2. At the beginning of a forming process, the stack of prepreg had a circular shape with a diameter of 140mm, and was packed between two diaphragms. The setups and forming parameters of experimental trials 3 and 4 were identical, except for the stack of prepreg plies. In Exp. Trial 3, the stack was 6-ply $[\pm 45, 0/90, \pm 45]_s$ of prepreg. Severe wrinkles developed in the flange of the formed part. Figure 3b shows a photograph of the formed part after it was removed from the diaphragm packing without curing. The wrinkles are visible, but, due to spring-back, are less severe than they were at the final stage of the forming. In Exp. Trial 4, the stack was laid up from 3-ply $[\pm 45, 0/90, \pm 45]$ of prepreg, and the part was formed without wrinkles.

In all four experimental trials, the stack of prepreg was covered by release films at both sides to avoid direct contact with diaphragms. At the beginning of a forming process, the release films were approximately of the same shape, and slightly larger than, the prepreg stack. At the end of a forming process, Figure 2c shows that when full vacuum was applied between the top and bottom diaphragms, the release films deformed as if stuck to the diaphragms. In comparison, when partial vacuum was applied between the diaphragms, the release film deformed as if stuck with the stack of prepreg. The deformation of release films in Exp. Trials 3 and 4 are not reported, but judging from photographs of similar tests (Young *et al*., 2001), they were likely to have stuck to diaphragms as well.

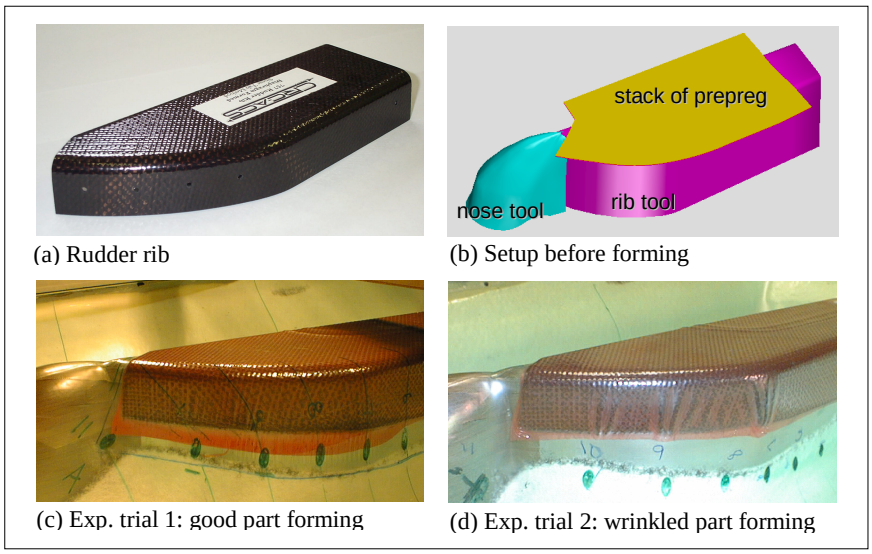

(a) Rudder rib (b) Setup before forming

(c) Exp. trial 1: good part forming (d) Exp. trial 2: wrinkled part forming

Figure 2. *Experimental trials of forming a rudder leading edge rib*

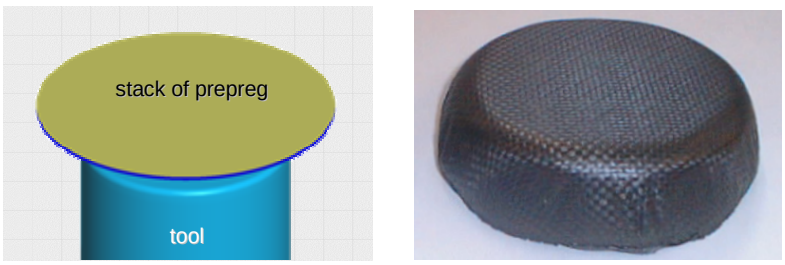

(a) Setup before forming (b) Exp. trial 3: wrinkled 6-ply cup forming

Figure 3. *Experimental trials of forming a simple cup shape*

3. Methodology for finite element simulations

3.1. *General features*

The 2002 version of PAM-FORM (ESI software, 2002) was chosen as the simulation tool, because of its capacity to handle non-linear large-sliding contact, and the specific in-built triple-phase shell element, namely Material 140, which was purposely developed to simulate viscous, non-orthogonal and large strain of fibre-reinforced composites.

In simulations, the forming box and tools were modelled by shell elements with null material properties, representing rigid body behaviour. The diaphragms were modelled separately by membrane elements. Each ply of prepreg was modelled, individually, by the Material 140 elements described above. To achieve a better description of the rate-independent component of the intra-ply shearing stiffness, each Material 140 element was overlapped by a membrane element, as previously described (Yu *et al*., 2000). The release films were treated as additional stiffness in neighbouring diaphragms in simulations of Exp. Trials 1, 3 and 4, or as additional stiffness in neighbouring prepreg plies in simulations of Exp. Trials 2.

Contact interfaces, catalogued in Table 2, were defined for each pair of neighbouring materials, or between materials with the potential to contact with each other. All sliding interactions at interfaces, except prepreg-to-prepreg, were described by Coulomb frictions with friction coefficients being measured from standard friction tests, or approximated from experimental results. The release-film-to-prepreg friction was approximated as Coulomb friction due to the lack of friction characterization data. A friction coefficient, $\mu_{RF/PREG}$, was determined as follows. At high pressures, about 47kPa and above, as in the Exp. Trial 1, the release films stuck with diaphragms and slid on prepregs so $\mu_{RF/PREG} < \mu_{RF/DIAPH}$ for this range of pressure. At lower pressures, about 38kPa and below, as in the Exp. Trial 2, the release films stuck with prepregs and slid on diaphragms so $\mu_{RF/PREG} > \mu_{RF/DIAPH}$ for this range of pressures. Assuming that the release film-to-prepreg friction at 95kPa is no less than that at 38kPa, it was deduced that $95\times\mu_{RF/PREG|95kPa} \geq 38\times\mu_{RF/PREG|38kPa} > 38\times\mu_{RF/DIAPH}$, so that at 95kPa pressure, $\mu_{RF/PREG} > 0.4\mu_{RF/DIAPH}$.

The vacuum processes, including the vacuuming level between the diaphragms and within the cavity of forming box, were modelled by loading histories of normal pressures applied to the top and bottom diaphragms. Considering that the PAM-FORM software makes use of an explicit solution algorithm that requires a small time step to ensure stability, the time duration of the real pressure history was scaled by 7.5e-5 in simulations. With this level of speed-up, no artificial inertia effects were observed in the simulations.

Table 2. *A summary of interfaces defined in the simulations*

Interface	Contact type	Frict. model	Friction coefficient
diaphragm/box	node-to-segment	Coulomb	set to a large value as a reasonable approximation
Diaphragm/tools	node-to-segment	Coulomb	measured by CRC-ACS
diaph + release film/prepreg*	segment-to-segment	Coulomb	written as $\mu_{RF/PREG}$, about $(0.4\sim1.0) \times \mu_{RF/DIAPH}$
diaph/release film + prepreg#	segment-to-segment	Coulomb	written as $\mu_{RF/DIAPH}$, measured by CRC-ACS
prepreg/prepreg	segment-to-segment	non-linear viscous	not applicable, see Section 3.3 for details

* applies to simulations of Exp. Trials 1, 3 and 4;
# applies to simulations of Exp. Trial 2.

3.2. *Modelling of diaphragms and release films*

The diaphragm materials, which were supplied in rolls, showed approximately 8% difference in apparent stiffness along the transverse and longitudinal directions. However for the sake of simplicity, isotropic elasto-plasticity was assumed in the simulations (Yu *et al.*, 2003b). The stress-strain curves of the diaphragm materials were measured from uniaxial tension tests, and were verified by inflation tests as shown in Figure 4.

Release films are weaker and thinner than diaphragm materials, therefore their stiffness was ignored in earlier simulations (Yu *et al.*, 2000). This study tries to evaluate the effects of release films, by adding additional stiffness to their neighbouring materials, as mentioned above. Due to the lack of material characterisation test results, the stress-strain curves of the release films were scaled from those of diaphragm materials by a factor, which was chosen to be 0.5 considering the tensile strength specified by the material vendor. Considering the thickness ratio in addition, the release film stiffness is about 16.7% of the diaphragm stiffness.

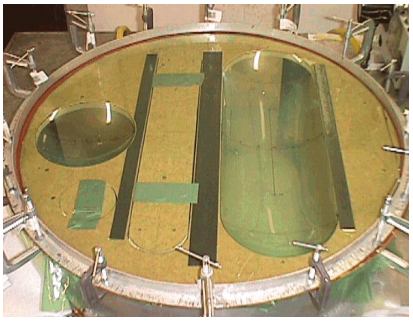

(a) Setup of inflation test

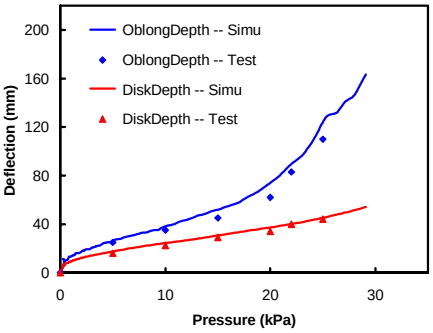

(b) Comparison between measurements and PAM-FORM simulations.

Figure 4. *Verification of diaphragm material properties by inflation tests*

3.3. *Modelling of an individual ply of woven fabric prepreg*

As pre-defined by the Material 140 shell element, an individual ply of woven fabric is decomposed into two directions according to their orientations. Each is assigned an axial stiffness that represents the equivalent Young's modulus of the prepreg along the fibre direction, and an out-of-plane bending stiffness that can be scaled by a bending factor to correlate with ply self-weight tests (Cartwright *et al.*, 1999). To ensure correct forming simulations, the Young's modulus does not need to be very accurate, but should be within a reasonable range.

The important property of a prepreg is the intra-ply shearing stiffness which resists trellis deformations. The Material 140 shell element addresses this stiffness based on a modified version of the ideal fibre reinforced fluid (IFRF) model (Spencer, 1972), treating the composite as a continuum of inextensible fibres within a purely viscoelastic matrix. This model was further modified in (Yu *et al.*, 2003a), by overlaying a rigid-plastic-hardening material onto the viscous fluid. Assuming isotropic viscosity, power law rate dependency and linear strain hardening, the constitutive relationship of the matrix, corresponding to Cauchy stress tensor, can be written as:

$$s_{ij} = 2\eta_0 \dot{\varepsilon}^{n-1} \dot{\varepsilon}_{ij} + \frac{2}{3}(a + b\varepsilon)\dot{\varepsilon}^{-1}\dot{\varepsilon}_{ij} \qquad [1]$$

where, s_{ij} and $\dot{\varepsilon}_{ij}$ are deviatoric stress and strain rate, respectively; η_0 and n are parameters for power law viscosity; $(a + b\varepsilon)$ is the von Mises equivalent stress, σ_s,

for rigid-plastic material under the assumption of linear hardening; ε and $\dot{\varepsilon}$ are the equivalent strain and strain rate, respectively.

A numerically more accurate model, the restrained membrane model, has also been proposed in (Yu *et al.*, 2003a). However, the simulations presented in this study are based on the modified IFRF model, Equation [1], because a recent verification study (Yu *et al.*, 2004c) revealed that the intra-ply shearing stiffness must be scaled up significantly, far more than the difference between the two models, in order to correlate a simulation with the experimental trial that formed a wrinkled part. The reason of such a level of intra-ply shearing stiffness scaling-up has not been clarified yet. It is postulated, and demonstrated by a modelling analysis, to be related with the compaction pressures on the prepreg in experimental forming trials but not in material characterization tests.

Equation [1] was built on multi-parameters, which makes the way to scale-up the intra-ply shearing stiffness non-unique. Previously (Yu *et al.*, 2004c), only one parameter, the initial yield stress, a, was scaled up. As tried, this approach failed to correlate simulations to all four experimental trials introduced in Section 2. The present study follows a different approach, which seems more consistent with the modelling analysis, *i.e.* to scale-up all three parameters, η_0, a and b, in Equation [1], simultaneously by one factor, f_G.

3.4. *Modelling of viscous friction of inter-ply sliding between prepregs*

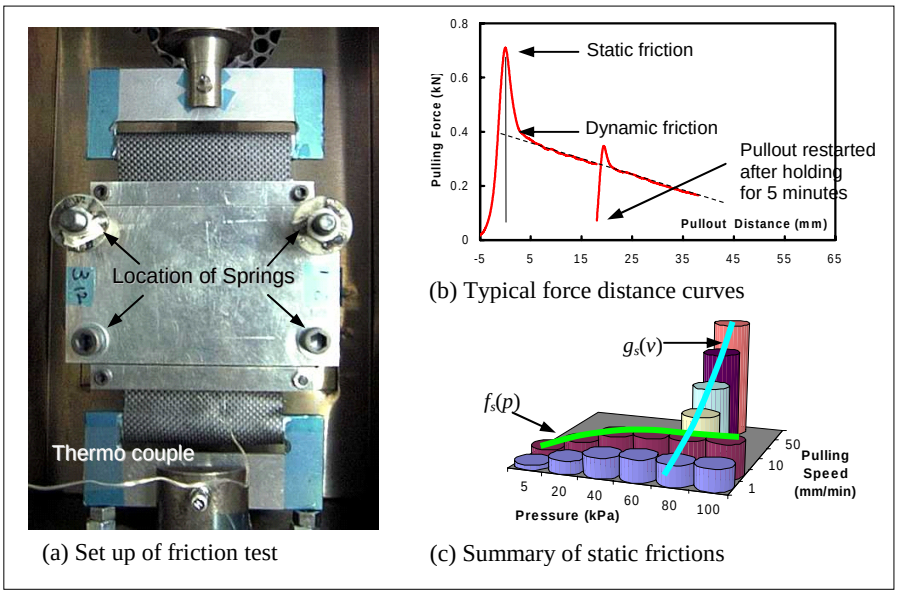

(a) Set up of friction test

(b) Typical force distance curves

(c) Summary of static frictions

Figure 5. *Setup and results of viscous friction test for inter-ply sliding*

The friction values used in the present simulations were measured by a test setup as shown in Figure 5a, previously detailed in (Yu, 2003). In brief, the setup was enclosed within an oven, and the compaction forces were applied using calibrated springs, through aluminium plates and rubber sheets, onto the prepregs. Figure 5b shows a typical relationship between pulling force and pullout distance measured at a constant pulling speed and under a constant compaction force. It can be seen that the pulling force has its maximum value at zero pullout. Once sliding initiated, it experienced a sharp decrease over about 5 mm of pullout distance, which was thereafter followed by a continued gradual decrease. The "gradual decrease" of pulling force can be attributed to the reduction of contact area due to ply pull out. However, the "sharp decrease" appears to be related to other mechanisms. As illustrated in the figure, it re-occurred, together with a preceding hump, when the pullout test was resumed after a hold for five minutes. This phenomenon leads to the definition of "static friction" and "dynamic friction", as illustrated in Figure 5b. Accordingly, the friction per unit contact area, F, at a certain pullout distance, can be expressed as Equation [2]:

$$F = \lambda F_s + (1-\lambda) F_d \qquad [2]$$

where, F_s and F_d are static and dynamic friction, respectively, per unit contact area. λ is a weight function representing the effects of pullout distance, which equals one at zero pullout, and zero after a certain distance of pullout. Both F_s and F_d are functions of pressure, p, and pulling velocity, v. As verified by available test results, the effects of pressure and velocity can be decomposed, so that,

$$F_s = f_s(p) g_s(v), \; F_d = f_d(p) g_d(v) \qquad [3]$$

where, the functions f_s and g_s, in relation to static friction, are defined as illustrated in Figure 5c. The functions f_d and g_d, in relation to dynamic friction, are defined in a similar approach.

In the present study, the viscous friction is incorporated via a user friction subroutine. As the sliding distance is currently not among the list of parameters passed into the user subroutine, the two extreme cases, *i.e.*, the static friction and the dynamic friction, were both tried in the simulations.

3.5. *Meshing technology to avoid intra-ply shear locking*

Nowadays, FE simulations of composite forming, including those using PAM-FORM software, are capable of tracing fibre directions, ensuring that non-orthogonal material axes are updated as the simulations progress. However, in general, such a simulation does not satisfy the correctness requirement when used with arbitrarily oriented meshes, due to a numerical problem termed intra-ply shear locking (Yu *et al.*, 2004a; 2004b). This intra-ply shear locking is not related with

physical fibre jamming, nor with constitutive modelling of fabric materials. Instead, it is the product of improper formulations of the element displacement field that fail to capture all essential deformation modes.

In respect to woven fabrics (Yu *et al*., 2004a), the essential intra-ply shear modes for an arbitrary 4-node element include one mode of uniform trellis deformation, and four modes of in-plane fibre bending. For an arbitrary 3-node element, those include one mode of uniform trellis deformation, and two modes of in-plane fibre bending. The number of essential modes reduces when the element orientation is less arbitrary. In an extreme case when all four boundaries of a 4-node element, or any two boundaries of a 3-node element, align with the fibre directions, the element has only one essential intra-ply shear mode, that is the uniform trellis deformation.

To the best knowledge of the authors, in-plane fibre bending has not been implemented at the element level in any commercial or in-house software package for composite forming simulations. This includes Material 140 element of PAM-FORM. As a result, an element can behave extremely overly stiffly in respect to the missing modes, or in the jargon of finite element analysis, this can lead to a phenomenon of numerical locking, which in the current situation is termed intra-ply shear locking (Yu *et al*., 2004a; 2004b). As demonstrated in the same references, the intra-ply shear locking explains the incorrect deformation profiles as well as the overly-estimated reaction forces in bias extension test simulations, and spurious wrinkles in composite forming simulations.

To avoid intra-ply shear locking, two approaches may be followed. One is to enhance element displacement and strain fields so that all essential intra-ply shear modes are properly implemented at the element level. The other is to reduce the number of essential intra-ply shear modes, by using aligned mesh technology, *i.e.* by aligning all boundaries of a 4-node element, and any two boundaries of a 3-node element, to fibre directions at the beginning of simulations. The alignment is then preserved throughout the progress of a simulation. Due to this alignment, the essential intra-ply shear mode of an element shrinks to the uniform trellis deformation, which has been well implemented in a number of elements including the Material 140 element of PAM-FORM. The effectiveness of the aligned mesh technology was verified in (Yu *et al*., 2004a), by a number of case studies, ranging from simple patch tests, to 2D simulations of bias extension tests, and to 3D simulations of the diaphragm forming of a simple cup shape. As an example, Figure 6 illustrates the effectiveness of the aligned mesh technology in solving the problem of intra-ply shear locking.

Aligned mesh technology was also adopted in the present study. Figure 7 shows the meshes of [0, 90] and [±45] plies in simulations of Exp. Trials 1 and 2. It can be seen that the meshes applicable for the composite forming simulations differ significantly from what may be suitable for metal forming simulations. Here, 3-node elements were used within the whole domain of the prepreg plies, because they do not incur the problem of hourglass mode deformations, which would

otherwise exist in a mesh constructed using regular 4-node elements when in-plane integration is performed at one Gauss point. In addition, 3-node elements do not experience the warp problem that is common to 4-node elements.

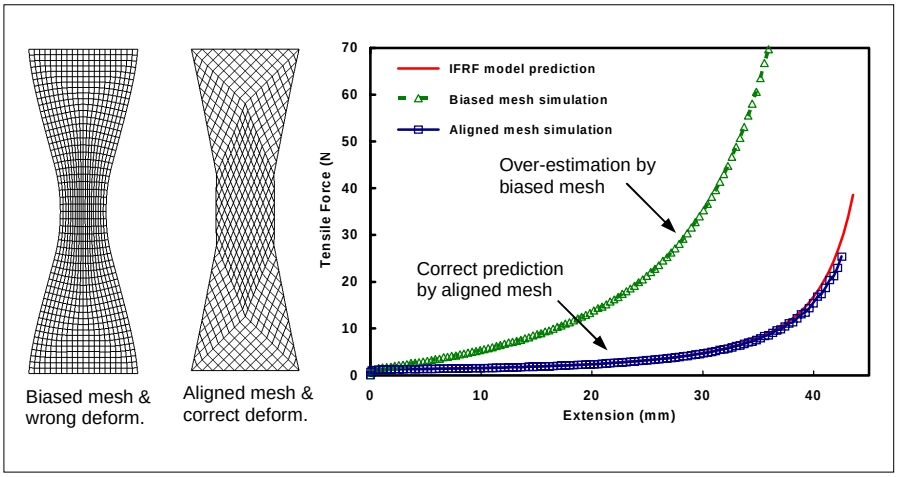

Figure 6. *Simulations of bias extension tests using biased and aligned meshes*

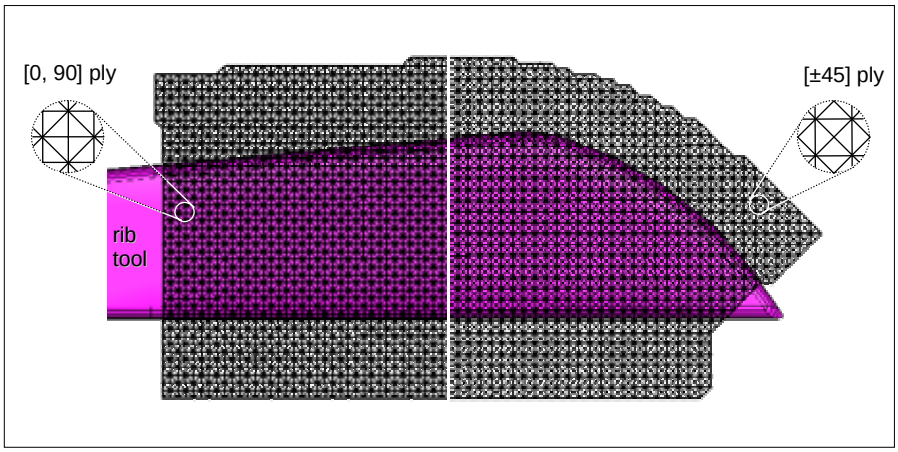

Figure 7. *Aligned meshs of 3-node elements in simulations of rib forming*

4. Simulation results

4.1. *Simulations that best correlate with experimental trials (SimuCase A)*

Due to the uncertainty in intra-ply shearing stiffness, and inaccuracy in release film stiffness, release-film-to-prepreg friction, and prepreg-to-pregreg friction, and to evaluate possible effects from simulation parameters, the present simulations have been performed using a large number of combinations of material and simulation parameters. This section introduces the simulations that best correlate with all four experimental trials. Sensitivity studies will be introduced in subsequent sections.

Table 3 summarizes the simulations that were performed with the following parameters, which are given a reference code "SimuCase A" for later reference:

– the release film stiffness equalled 16.7% of diaphragm stiffness. Here stiffness is defined as true stress multiplied by thickness at given plastic strain;

– the friction coefficient of the release-film-to-prepreg interface took the value measured at the diaphragm-to-release film interface, *i.e.*, $\mu_{RF/PREG} = \mu_{RF/DIAPH}$;

– the preprep-to-prepreg friction was calculated based on the static friction, F_s, with the ply-to-ply contact penalty $k_0 = 0.005$;

– the scale-up factor, f_G, was determined inversely as listed in Table 3.

Table 3. *Parameter studies to best correlate simulations with experimental trials*

Exp. Trials	$f_G = 2$	$f_G = 4$	$f_G = 6$	$f_G = 8$	$f_G = 10$	$f_G = 12$	$f_G = 14$
1. rib, good	←	←	←	←	Y	M	N
2. rib, wrinkled	N	M	Y	Y	Y	→	→
3. cup, wrinkled	←	←	N	Y	Y	→	→
4. cup, good	←	←	←	←	Y	N	→

* Y/N: simulation agrees / disagrees with experimental trial; M: between Y and N;
←/→: results at the right / left column can be carried over with full confidence

The results presented in Table 3 reconfirm the necessity to significantly scale-up the intra-ply shearing stiffness, in order to correlate simulations with experimental trials, (here Exp. Trials 2 and 3) that produced wrinkled parts. Meanwhile, excessive scaling-up needs also be avoided, in order to correlate simulations with the experimental trials, (here Exp. Trials 1 and 4) that produced non-wrinkled parts. As a result, to correlate with all four experimental trials, f_G can only vary between 8 to 10. This level of scaling-up is well supported by a modelling analysis (Yu *et al.*,

2004c) that included the compaction pressure as a factor in intra-ply shearing stiffness. In pullout tests of the same material, the friction increases to nine times as high when compaction pressure varies from zero to the range of 60 to 100 kPa. This gives further confidence in the value of f_G between 8 and 10.

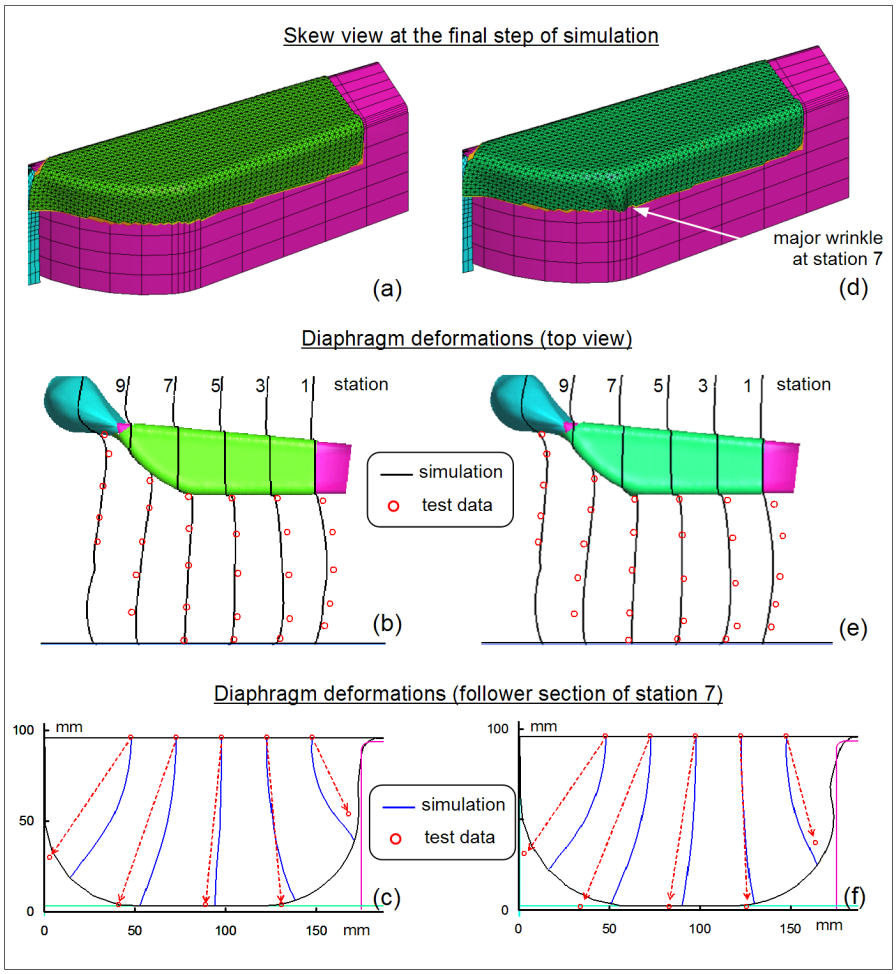

Figure 8. *Simulation (SimuCase A, f_G = 10) results of Exp. Trials 1 and 2. (a) to (c) correspond to Exp. Trial 1, (d) to (e) correspond to Exp. Trial 2*

Figure 8 presents the simulation results of Exp. Trials 1 and 2, obtained with SimuCase A simulation parameters and a further specification of f_G = 10. In agreement with the experimental results, a non-wrinkled part was predicted for Exp. Trial 1, and a wrinkled part was predicted for Exp. Trial 2, see Figure 8a and 8d, respectively. Figures 8b, c, e and f compare the predicted deformations of the top

diaphragm with those measured at the experimental trials. Reasonable agreements were achieved. It is noted that, when f_G varies from 1 to 10, pictures shown in Figure 8a to 8c are hardly changed, and those shown in Figure 8d to 8e are only slightly affected except over the wrinkled area.

Figure 9 presents the simulation results of Exp. Trials 3 and 4, obtained with simulation parameters the same as those introduced for Figures 8. The likelihood of wrinkle development agrees well between the predictions and experimental trials.

4.2. *Effects of release film stiffness (SimuCase B)*

Two sub-cases were investigated, as listed in Table 4. The simulation parameters were the same as those in SimuCase A, except that the release film stiffness was set at zero in SimuCase B0, and 67.7% of the diaphragm stiffness in SimuCase B4.

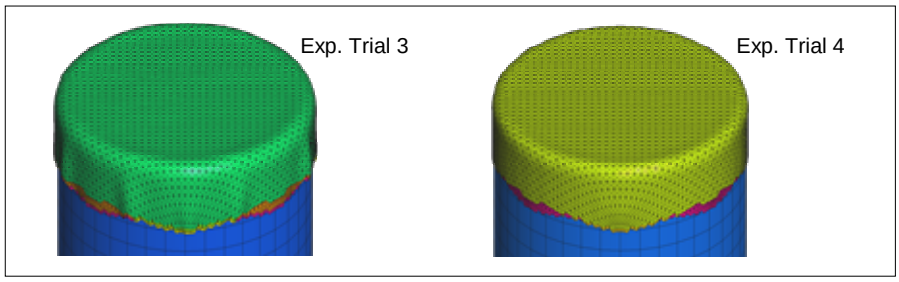

Figure 9. *Simulation (SimuCase A, f_G = 10) results of Exp. Trials 3 and 4*

Table 4. *The effects of release film stiffness*

Experimental Trials	SimuCase B0, f_G = …				SimuCase B4, f_G = …				
	6	8	10	14	1	6	7	8	10
1. rib, good	←	←	Y	N	Y	Y	M	N	N
2. rib, wrinkled	N	--	Y	→	Y	Y	→	→	→
3. cup, wrinkled	--	Y	Y	→	←	N	M	Y	Y
4. cup, good	←	←	Y	N	←	←	←	Y	Y

* see Table 3 for notes of Y/N/M, and ←/→.

The effect of release film stiffness is case-dependent. The most significant effect on wrinkle prediction was observed in simulations of Exp. Trial 2, where release films were stuck to prepregs. With a higher release film stiffness, the wrinkle was

predicted at lower f_G. A similar but weaker trend was observed in simulations of Exp. Trial 1. No effects were identified in simulations of Exp. Trials 3 and 4.

In SimuCase B0, f_G = 10 is still the best fit value to correlate simulations to all four experimental trials. In SimuCase B4, no suitable f_G exists, because the value that is high enough to predict wrinkles for Exp. Trial 3 is simply too high to predict good part for Exp. Trial 1. This study shows that the release film stiffness assumed in SimuCase A, of 16.7% of diaphragm stiffness, is reasonable.

4.3. *Effects of release-film-to-prepreg friction (SimuCase C)*

This case study applies to simulations of Exp. Trials 1, 3 and 4. The simulation parameters were the same as those specified in SimuCase A, except that $\mu_{RF/PREG}$ equals $0.4\mu_{RF/DIAPH}$, the lower bound of the possibility. No changes were observed on the likelihood of wrinkle prediction. When $\mu_{RF/PREG}$ was further reduced to $0.01\mu_{RF/DIAPH}$, which was far beyond the reasonable range, the predicted wrinkles become slightly less severe, or disappear. This shows that within a reasonable range, $\mu_{RF/PREG}$ does not affect the wrinkle prediction.

4.4. *Effects of contact penalty for prepreg-to-prepreg interface (SimuCase D)*

This case study investigates the robustness of the penalty value within the range that was traditionally regarded as acceptable, *i.e.* neither penetration nor severe noise existed. The simulation parameters were the same as those in SimuCase A, except that the contact penalty for the prepreg-to-prepreg interface equals $0.6k_0$ in SimuCase D1, and $0.2k_0$ in SimuCase D2. It was found that a lower value of contact penalty led to more likelihood of wrinkle prediction. This effect is more significant in simulations of Exp. Trial 1 than in those of Exp. Trial 3. As a result, no f_G value that suits both trials can be identified.

This study raised a question on the role of the contact penalty as well as the trustworthiness of the simulation results. Further studies were therefore performed on simulations of double-diaphragm 3-ply pullout tests. It was revealed that normal contact forces were not affected by the value of contact penalty, and that lower friction forces resulted from a lower value of the contact penalty, and that for Coulomb friction, the effects of contact penalty did not exist. Figure 10 explains the possible mechanism behind this. In short, the segment-to-segment contact type applied in the present study is a dual-searching approach, so both the pressure and friction are calculated as the sum of the two searches. Due to the requirement of normal force balance, the pressure calculation is always correct in the current situation. But the friction calculation is something different. At low contact penalty, the pressures associated with the two searches are almost the same therefore correct friction can be calculated. At high penalty contact, the pressures do not equal and a lower friction is predicted as illustrated in the figure. The phenomenon only occurs

when the friction *versus* pressure relationship is nonlinear, hence these contact penalty effects do not exist with Coulomb friction.

Because the contact penalty adopted in SimuCase A is at the high bound, we need to check whether the so-induced artificial under-estimation of friction is within the reasonable range. This is performed in the next section.

4.5. *Effects of prepreg-to-prepreg friction (SimuCase E)*

The simulation parameters used in this case study were the same as SimuCase A, except that the contact penalty of prepreg-to-prepreg interface was $0.2k_0$, the lower bound that nearly ensured correct friction prediction, and that dynamic friction instead of static was used for prepreg-to-prepreg friction calculation.

The results agree well with those obtained in SimuCase A, except that for Exp. Trial 1 at $f_G = 12$, SimuCase E predicted no wrinkles while SimuCase A predicted a marginal wrinkle. This means that the prepreg-to-prepreg frictions calculated in SimuCase A are very close to, and a little bit higher than, those in SimuCase E. In view of this, all simulations presented in Sections 4.1 to 4.4 are regarded as valid. It however needs to be noted that the *real* inter-ply frictions reached in the simulations are very close to the dynamic frictions.

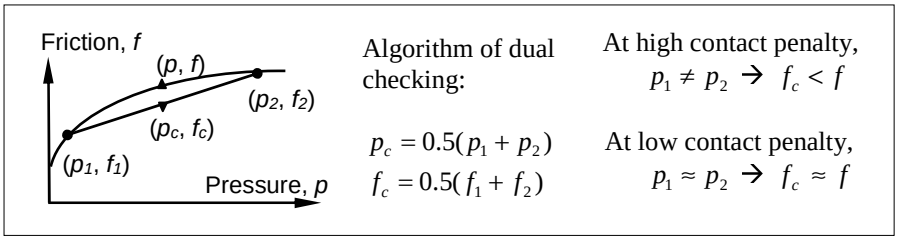

Figure 10. *A proposed explanation of contact penalty effect on friction calculation*

5. Final remarks

This study evaluated finite element simulations of diaphragm forming processes, through a comprehensive approach. Although some material and simulation parameters were determined by a reverse engineering approach, the combination of four experimental trials, on which these back-calculations were based, is well-conditioned because of their distinct wrinkle/no-wrinkle features associated with different setups. The parameters applying to the best-match simulations are within a reasonable range. By using a single set of material and simulation parameters, the simulations are well correlated with all four experimental trials, indicating a high level reliability of the simulations.

In addition, the simulations re-confirm the necessity to scale-up the intra-ply shearing stiffness from what was measured in bias extension tests without compaction pressures. The level of scaling-up is supported by a modelling analysis. Further experimental work is needed to provide thorough clarification of this issue. The simulations also highlight the effects of contact penalty on calculations of non-Coulomb frictions, and the sensitivity to inter-ply friction. A more accurate algorithm for friction calculation is therefore desirable.

Acknowledgements

This work was supported by the Australian government under the ARC-Linkage Project Scheme, and the AusIndustry R&D Tax Concession/Offset Scheme, and by ESI Group who provided a copy of the PAM-FORM software. The help from Allen Chhor of Pacific ESI and Patrick de Luca of ESI Software was invaluable.

6. References

Boisse P., Gasser A., Hivet G., "Analyses of fabric tensile behavior: determination of the biaxial tension-strain surfaces and their use in forming simulations", *Compos. Part A*, Vol. 32, No. 10, 2001, pp. 1395-1414.

Bibo G.A., Paton R., Development of the double diaphragm forming process for a rudder leading edge rib, TM 00007, 2000, CRC-ACS.

Cartwright B., deLuca P., Wang J., Stellbrink K., Paton R., "Some proposed experimental tests for use in finite element simulation of composite forming", *12th Int. Conf. on Compos. Mater*., 5-9 July 1999, Paris/France, paper 582, pp. 377- 89.

Cartwright B., Chhor A., Howlett S., McGuckin D., Paton R., Ye L., Yu X., "Industrially robust modelling of viscous friction effects in composites", *EuroPAM 2003*, October 16-17, 2003, Mainz, Germany.

Cao J., Xue P., Peng X.Q., Krishnan N., "An approach in modeling the temperature effect in thermo-stamping of woven composites", *Compos. Struct.*, Vol. 61, No. 4, 2003, pp. 413-20.

Crossthwaite M., Cartwright B., Paton R., Experimental data to verify PAM-FORM modelling of the double diaphragm forming process, 2000, CRC-ACS.

de Luca P., Lefébure P., Pickett A.K., "Numerical and experimental investigation of some press forming parameters of two fibre reinforced thermoplastics: APC2-AS4 and PEI-CETEX", *Compos. Part A*, Vol. 29, No. 1-2, 1998, pp. 101-10.

Dong L., Lekakou C., Bader M.G., "Processing of composites: Simulations of the draping of fabrics with updated material behaviour law", *J. Compos. Mater.*, Vol. 35, No. 2, 2001, pp. 138-63.

ESI Software, PAM-FORM 2002 Solver Reference Manual, 2002.

Laroche D., Vukhanh T., "Forming of Woven Fabric Composites," *J. Compos. Mater.*, Vol. 28, No. 18, 1994, pp. 1825-39.

Long A.C., Souter B.J., Robitaille F., Rudd C.D., "Modelling the effects of fibre architecture on reinforcement fabric deformation", *Plastics Rubber Composites*, Vol. 31, No. 2, 2002, pp. 87-97.

Mair R.I., "Advanced composite structures research in Australia", *Compos. Struct.*, Vol. 57, No. 1-4, 2002, pp. 3-10.

Spencer A.J.M., *Deformation of Fibre-Reinforced Materials*, Oxford: Clarendon Press, 1972.

VanWest B.P., Pipes R.B., Keefe M., Advani S.G., "The draping and consolidation of commingled fabrics", *Compos. Manufact.*, Vol. 2, No. 1, 1991, pp. 9-22.

Wang, J., Paton R., Page J.R., Forming properties of thermoset fabric prepregs at room and elevated temperature, TM 97028, 1997, CRC-ACS.

Young M., Paton. R., Investigation on the forming of a simple cup, TM01003, 2001, CRC-ACS.

Young M., Diaphragm forming guidelines, TM 03016, 2003, CRC-ACS.

Yu X., Cartwright B., Zhang L., Mai Y.-W., Paton R., "Finite element simulations of the diaphragm forming process", *15th Annual Tech. Conf. of the American Society for Composite*, 2000, Texas, USA.

Yu X., Experimental study of the interplay shearing resistance, TM 03009, 2003, CRC-ACS.

Yu X., Zhang L., Mai Y.-W., "Modelling and finite element treatment of intra-ply shearing of woven fabric", *J. Mater. Processing Tech.*, Vol. 138, No. 1-3, 2003a, pp. 47-52.

Yu X., Zhang L., Mai Y.-W., PAM-FORM simulations of the double diaphragm forming process, TM 03059, 2003b, CRC-ACS.

Yu X., Cartwright B., McGuckin D., Ye L., Mai Y.-W., "Intra-ply shear locking in finite element analyses of woven fabric forming processes", *Compos. Part A*, 2004a, submitted.

Yu X., Ye L., Mai Y.-W., "Finite element spurious wrinkles on the thermoforming simulation of woven fabric reinforced composites", *ESAFORM2004*, 2004b, Trondheim, Norway.

Yu X., Ye L., McGuckin D., "Evaluation of intra-ply shearing stiffness for a plain weave fabric prepreg.," *ACCM-4*, July 2004c, Sydney, Australia.